

SPECIAL
ISSUE

Structure–Activity Relationships on Cinnamoyl Derivatives as Inhibitors of p300 Histone Acetyltransferase

Valentina Noemi Madia,^[a] Rosaria Benedetti,^[b] Maria Letizia Barreca,^[c] Liza Ngo,^[d] Luca Pescatori,^[a] Antonella Messori,^[a] Giovanni Pupo,^[a] Francesco Saccoliti,^[a] Sergio Valente,^[a] Antonello Mai,^[a] Luigi Scipione,^[a] Yujun George Zheng,^[d] Cristina Tintori,^[e] Maurizio Botta,^[e] Violetta Cecchetti,^[c] Lucia Altucci,^[b, f] Roberto Di Santo,^[a] and Roberta Costi^{*[a]}

Human p300 is a polyhedral transcriptional coactivator that plays a crucial role in acetylating histones on specific lysine residues. A great deal of evidence shows that p300 is involved in several diseases, including leukemia, tumors, and viral infection. Its involvement in pleiotropic biological roles and connections to diseases provide the rationale to determine how its modulation could represent an amenable drug target. Several p300 inhibitors (i.e., histone acetyltransferase inhibitors, HATIs) have been described so far, but they all suffer from low potency, lack of specificity, or low cell permeability, which thus highlights the need to find more effective inhibitors. Our cinnamoyl

derivative, 2,6-bis(3-bromo-4-hydroxybenzylidene)cyclohexanone (RC56), was identified as an active and selective p300 inhibitor and was proven to be a good hit candidate to investigate the structure–activity relationship toward p300. Herein, we describe the design, synthesis, and biological evaluation of new HATIs structurally related to our hit; moreover, we investigate the interactions between p300 and the best-emerged hits by means of induced-fit docking and molecular-dynamics simulations, which provided insight into the peculiar chemical features that influence their activity toward the targeted enzyme.

Introduction

Described for the first time as an adenoviral E1A-binding protein,^[1] p300/CBP is part of the histone acetyltransferase (HAT)

enzyme family together with another four families, including GCN5-related *N*-acetyltransferase (GNAT), MYST, nuclear receptor coactivators, and TATA-binding protein (TBP)-associated factor TAF_{II}.^[2] p300 acts primarily as a histone acetyltransferase and has the ability to transfer an acetyl group from acetyl-coenzyme A (Ac-CoA) to the histone ϵ -NH₂ group of the lysine side chain as a means to remodel chromatin to a relaxed superstructure. This modification results in a change in histone–DNA and histone–protein interactions. Histone acetylation can occur in promoter regions, at which p300 acts as a transcription cofactor for a variety of nuclear proteins (including oncoproteins,^[3] viral proteins,^[4] and tumor-suppressor proteins^[5]), or over large regions of chromatin, and it affects global gene expression levels.^[6] p300 substrates are not limited to histone proteins but include more than 75 different proteins.^[7] Notably, the acetylation activity of p300 can also be addressed to viral proteins such as HIV-1 integrase, which contributes significantly to viral replication.^[8] Moreover, an extensive autoacetylation process occurs in an intermolecular fashion, which regulates the activation state and the mediated transcriptional regulation of p300.^[9]

By acetylating different substrates, p300 is implicated in a wide array of cellular processes, such as cell-cycle regulation,^[10] differentiation,^[11] and DNA damage response,^[12] and it can promote opposite cellular outcomes such as proliferation and apoptosis.^[13] Because of the biological importance of p300, alteration of the gene sequence (mutation, chromosomal translocation, and dysregulation) is correlated to many disease

[a] Dr. V. N. Madia, Dr. L. Pescatori, Dr. A. Messori, Dr. G. Pupo, Dr. F. Saccoliti, Dr. S. Valente, Prof. A. Mai, Dr. L. Scipione, Prof. R. Di Santo, Dr. R. Costi
Dipartimento di Chimica e Tecnologie del Farmaco, Istituto Pasteur-Fondazione Cenci Bolognetti, "Sapienza" Università di Roma, P.le Aldo Moro 5, 00185, Roma (Italy)
E-mail: roberta.costi@uniroma1.it

[b] Dr. R. Benedetti, Prof. L. Altucci
Dipartimento di Biochimica, Biofisica e Patologia generale, Università degli Studi della Campania Luigi Vanvitelli, Vico L. De Creschio 7, 80138, Napoli (Italy)

[c] Prof. M. L. Barreca, Prof. V. Cecchetti
Department of Pharmaceutical Sciences, University of Perugia, Via A. Fabretti 48, 06123 Perugia (Italy)

[d] Dr. L. Ngo, Prof. Y. G. Zheng
Department of Pharmaceutical and Biochemical Sciences, University of Georgia, Athens, GA, 30602 (USA)

[e] Dr. C. Tintori, Prof. M. Botta
Dipartimento di Biotecnologie, Chimica e Farmacia, Università degli Studi di Siena, Via Aldo Moro 2, 53100, Siena (Italy)

[f] Prof. L. Altucci
Istituto di Genetica e Biofisica, IGB "Adriano Buzzati Traverso", Via P. Castellino 111, 80131, Napoli (Italy)

Supporting Information and the ORCID identification number(s) for the author(s) of this article can be found under:
<http://dx.doi.org/10.1002/cmdc.201700040>.

This article is part of a Special Issue on the XXIV National Meeting in Medicinal Chemistry (NMMC 2016, Perugia, Italy). To view the complete issue, visit: <http://onlinelibrary.wiley.com/doi/10.1002/cmdc.v12.16/issueoc>.

conditions, including cancer,^[14] chronic neuropathic pain,^[15] and cognitive and neurodegenerative disorder.^[16] Most recently, implication of p300 was also described in ventricular remodeling after myocardial infarction.^[17]

p300 is characterized by highly conserved regions that can be distinguished by four different functional domains: one, a catalytic HAT domain, in which histone and protein acetylation occurs; two, four recognized transactivation domains that mediate protein–protein interactions with DNA-binding transcription factors and transcription machinery; three, the bromodomain, which recognizes histone acetylated tails; four, the cysteine–histidine-rich region. Recently, mutagenesis studies and resolution of the structure of the semisynthetic heterodimeric p300 HAT domain in complex with Lys-CoA revealed the catalytic mechanism of p300, for which the Tyr1467 and Trp1436 residues were shown to play a significant role in the acetylation reaction.^[18] Tyr1467 was reported to guide and protonate the sulfur atom of Ac-CoA, whereas Trp1436 was described to orient the lysine side chain for nucleophilic attack of the Ac-CoA cofactor. More recently, the resolution of the crystal structure of the p300 HAT domain bound to Ac-CoA confirmed this hypothesis and gave insight into the design of p300 inhibitors.^[19]

Owing to its relevant role in different pathological conditions, HAT p300 is considered an amenable target, and its modulation holds promise for future therapeutic strategies.^[20] The p300 inhibitors (i.e., HAT inhibitors, HATIs) so far described comprise natural compounds, some of them supplied from dietary plants (e.g., anacardic acid,^[21] curcumin,^[22] garcinol,^[23] epigallocatechin-3-gallate,^[24] and plumbagin)^[25] and synthetic small molecules (e.g., Lys-CoA,^[26] C646,^[27] isothiazolones,^[28] and cinnamoyl compounds).^[29]

Nevertheless, in the field of HATIs, a huge investigation margin is left owing to the necessity to find other inhibitors endowed with good pharmacokinetic and pharmacodynamic

profiles and to establish the exact inhibition mode toward p300. In the last decade, our research group was involved in the identification of HATIs,^[29] and among them, RC56 [2,6-bis-(3-bromo-4-hydroxybenzylidene)cyclohexanone] was identified as the most active and selective p300 inhibitor; it showed cellular activity by down regulation of the histone H3 acetylation level. Most recently, RC56 was used as an investigation tool to evaluate the acetylation level in H3K4 by p300 and the expression of the multidrug resistance (MDR1) gene in drug-resistant and drug-sensitive breast carcinoma cell lines.^[30] We considered RC56 a good hit candidate to investigate the structure–activity relationship toward p300. Herein, we report the design of new HATIs **1 a–s** and **2 a** by addressing six modifications to the RC56 structure involving both the benzylidene moiety and the central cyclohexanone portion to evaluate the role of the arylidene substituents, the central ring, and the carbonyl group in inhibiting the enzymatic target. In particular, 1) the bromine atom in the 3-position of the benzylidene portion was substituted with other atoms or groups: F (**1 b**), Cl (**1 c**), I (**1 d**), methyl group (**1 g**), hydroxy group (**1 e**), hydrogen atom (**1 a**), and phenyl ring (**1 f**); 2) the hydroxy group in the 4-position of the benzylidene portion was substituted with a bromine atom (**1 h**); 3) a third substituent in the 5-position of the benzylidene portion (Br, F, Cl) was introduced (**1 i**, **1 j**); 4) the cyclohexanone was reduced to cyclohexanol (**2 a**); 5) a carboxylic acid function was introduced in the 4-position of the cyclohexanone ring (**1 k**, **1 l**); 6) the cyclohexanone was substituted with a five-membered ring (**1 m**) or tetrahydrothiopyranone (**1 n**) and piperidinone (**1 o–s**) heterocycles. Thus, we report the synthesis and biological evaluation of HATI **1 a–s** and **2 a** (Table 1). All the synthesized compounds were tested on recombinant p300 by using an in vitro radiometric assay. Cell-based assays were performed with the most promising compounds to corroborate and strengthen the activities. Moreover, theoretical investigation of the interactions between p300 HAT and the

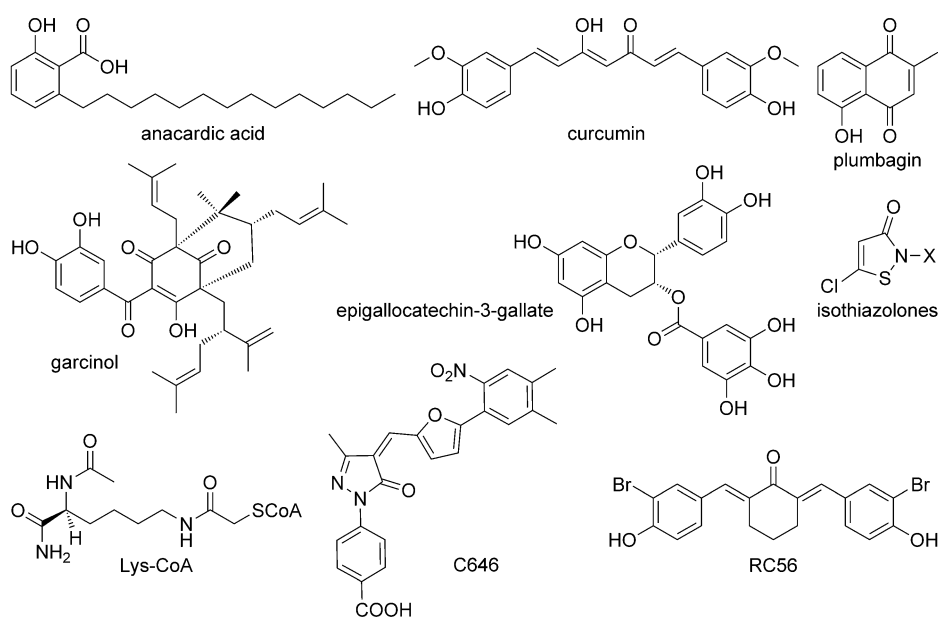
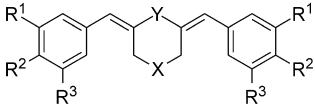


Table 1. p300 inhibitory activity of compounds **1 a–s** and **2 a** in enzyme assays.


Compd	X	Y	R ¹	R ²	R ³	Retaining activity [%] ^[a]	IC ₅₀ [μM] ^[b]
1 a	CH ₂	C=O	H	OH	H	28.6	
1 b	CH ₂	C=O	F	OH	H	6.3	38.9 ± 10.1
1 c	CH ₂	C=O	Cl	OH	H	7.7	45.5 ± 9.8
1 d	CH ₂	C=O	I	OH	H	5.8	8.1 ± 2.1
1 e	CH ₂	C=O	OH	OH	H	89.0	
1 f	CH ₂	C=O	Ph ^[c]	OH	H	92.2	
1 g	CH ₂	C=O	CH ₃	OH	H	3.0	26.8 ± 11.2
1 h	CH ₂	C=O	Br	Br	H	85.1	
1 i	CH ₂	C=O	Br	OH	Br	0	2.3 ± 0.5
1 j	CH ₂	C=O	F	OH	Cl	41.1	
1 k	CH ₂ CO ₂ H	C=O	CO ₂ H	OH	H	70.1	
1 l	CH ₂ CH ₂ CO ₂ H	C=O	OH	OH	H	128	
1 m	0	C=O	Br	OH	H	41.2	
1 n	S	C=O	Br	OH	H	7.13	35.0 ± 12.3
1 o ^[d]	NH	C=O	OH	OH	H	114	
1 p ^[d]	NHCH ₃	C=O	OH	OH	H	82.4	
1 q ^[d]	NHCH ₂ CH ₃	C=O	NO ₂	OH	H	128	
1 r ^[d]	NHCH ₂ Ph	C=O	OH	OH	H	19.4	
1 s ^[d]	NHCH ₂ Ph	C=O	Br	OH	H	81.6	
2 a	CH ₂	CHOH	Br	OH	H	12.5	
RC56	CH ₂	C=O	Br	OH	H	0	30.9 ± 8.2
C646							3.6 ± 0.6

[a] Activity of p300 in the presence of 100 μM inhibitor, relative to positive control, which has no inhibitor. [b] Determined from dose–response curves; data are the mean ± SD of at least duplicates. [c] Phenyl. [d] Compound tested as its HCl salt.

best-emerged hits (i.e., **1 d** and **1 i**) was performed by means of induced-molecular-modeling experiments.

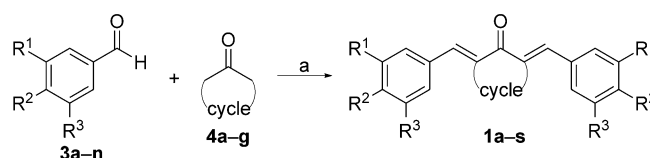
Results and Discussion

Chemistry

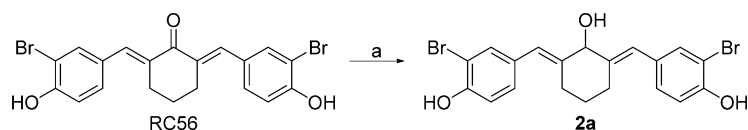
Bis-arylidene derivatives **1 a–s** were obtained by microwave-assisted (for **1 a–j**, **1 m**, and **1 n**) or acid-catalyzed (for **1 k**, **1 l**, and **1 o–s**) condensation of the appropriate five- or six-membered cycle (see Table 1) with the appropriate benzaldehyde following a previously reported synthetic approach (Scheme 1).^[29,31] Derivative **2 a** was obtained by reduction of the carbonyl group of RC56 to a hydroxy group in the presence of lithium aluminum hydride (Scheme 2). All the benzaldehydes used as starting materials were commercially available, except for **3 d** and **3 f**. Benzaldehyde **3 d** was obtained as reported in Azoulay et al.,^[32] whereas **3 f** was synthesized by a Suzuki coupling reaction (Scheme 3).

Biological evaluation

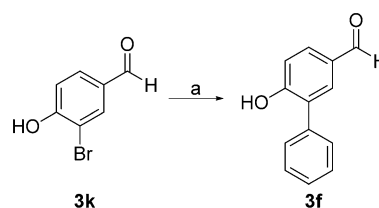
Newly synthesized compounds **1 a–s** and **2 a** could be categorized according to the nature of the central cycle (cyclohexanone derivatives **1 a–l**, cyclopentanone derivative **1 m**, tetrahydrothiopyranone derivative **1 n**, piperidinone derivatives **1 o–s**, and cyclohexanol derivative **2 a**). All of the compounds were tested against recombinant p300 (0.025 μM) by using the stan-



Scheme 1. Key synthetic step for the synthesis of bis-arylidene derivatives **1 a–s**. Reagents and conditions: for **1 a–j**, **1 m**, **1 n**: a) Montmorillonite K-10, 100 W, 100 °C, 5 min; for **1 k–l** and **1 o–s**: a) HCl_(aq), CH₃CO₂H, RT, 48 h.



Scheme 2. Synthesis of derivative **2 a**. Reagents and conditions: a) THF, LiAlH₄, 0 °C → RT, 2 h, 32%.



Scheme 3. Preparation of benzaldehyde **3 f**. Reagents and conditions: a) PhB(OH)₂, Pd(PPh₃)₄, Ba(OH)₂·8H₂O, 1,2-dimethoxyethane/H₂O, reflux, 4 h, 32%.

standard filter binding assay. Conditions for this assay included 100 μM H3-20 peptide and 1 μM [^{14}C] Ac-CoA with incubation at 30 $^{\circ}\text{C}$ for 6 min (Table 1). The activity of p300 was measured in the presence of the individual compounds, each at a fixed concentration of 100 μM . The positive control contained no inhibitor. The activity of each inhibitor solution was compared with that of the positive control to calculate the percentage of p300 retaining activity, which was the quantitative representation of the potency of each inhibitor. The IC_{50} values were further determined for those compounds showing less than 10% of p300 retaining activity at 100 μM (i.e., compounds **1b–d**, **1g**, **1i**, and **1n**). RC56 was found previously by us to be a potent p300 inhibitor and, thus, was used as the reference compound. In this experiment, RC56 revealed an IC_{50} value of 30.9 μM , which is six times greater than that already reported.^[29] The difference in the IC_{50} values of RC56 was attributed to altered assay conditions. In the previous study, the GST-p300 HAT domain was used to acetylate a histone protein mixture with [^{14}C] Ac-CoA as cofactor. The acetylated products were visualized by phosphorimaging after SDS-PAGE separation. In the present study, tag-free p300 was used as the enzyme source, and a high concentration of H3 peptide was used as the substrate. The reaction yields were controlled under the initial reaction conditions (product conversion typically was less than 20%).

Among the tested compounds, cyclohexanone derivative **1i** was the most active, and it showed complete inhibition to p300 activity at 100 μM . Its IC_{50} value was measured to be $(2.3 \pm 0.5) \mu\text{M}$, which is 15 times lower than that of RC56 [$(30.9 \pm 8.2) \mu\text{M}$]. Of note, we also measured the IC_{50} value of C646 to be $(3.6 \pm 0.6) \mu\text{M}$ under the same conditions. C646 is regarded as one of the most potent p300 inhibitors.^[27] Therefore, the potency of **1i** is at the same level as that of C646.

Among cyclohexanone derivatives **1a–l**, we discuss the preliminary structure–activity relationships according to the substituents on the benzylidene portion. Substitution of the bromine atom of RC56 with a hydrogen atom (as in **1a**), a hydroxy group (as in **1e**), and a phenyl ring (as in **1f**) resulted in a decrease in the inhibitory activity (residual acetylation: 28.6, 89.0, and 92.2%, respectively). Substitution of the bromine atom of RC56 with other halogen atoms (as in **1b–d**) as well as with a methyl group (as in **1g**) led to compounds with good inhibitory activity. In fact, compounds **1b**, **1c**, and **1g** showed IC_{50} values similar to that of RC56 ($\text{IC}_{50} = 38.9, 45.5,$ and $26.8 \mu\text{M}$, respectively). Notably, substitution of the bromine atom of RC56 with an iodine atom (as in **1d**) led to a compound that was five times more active ($\text{IC}_{50} = 8.1 \mu\text{M}$). The introduction of a second bromine atom on the benzylidene portion (as in **1i**) generated the most potent compound ($\text{IC}_{50} = 2.3 \mu\text{M}$), and conversely, substitution of the two bromine atoms of **1i** with fluorine and chlorine atoms (as in **1j**) decreased the activity (residual acetylation: 41.1%). The biological data also suggest a key role of the hydroxy groups on the benzene rings, as highlighted by comparison between RC56 ($\text{IC}_{50} = 30.9 \mu\text{M}$) and derivative **1h** (residual acetylation: 85.1% at 100 μM).

The cyclohexanone and tetrahydrothiopyranone derivatives showed similar activities (RC56 and **1n**, $\text{IC}_{50} = 30.9$ and $35.0 \mu\text{M}$,

respectively), whereas substitution of the cyclohexanone ring with cyclopentanone (as in **1m**), piperidinone (as in **1o–s**), and cyclohexanol (as in **2a**) led to a decrease in the inhibition potency (residual acetylation: 12.5 to 128%).

Among the piperidinone series featuring a 3,4-dihydroxybenzylidene substitution pattern, **1o**, **1p**, and **1r**, the most active compound was *N*-benzyl-substituted piperidinone **1r**. In this series, the introduction of a benzyl group in the 4-position of the piperidinone ring to give **1r** increased the inhibition potency relative to that of unsubstituted counterpart **1o** (residual acetylation: 19.4 and 114%, respectively). Moreover, comparing derivative **1r** with analogue **1s**, characterized by substitution of the hydroxy group in the 3-position of the benzylidene ring with a bromine atom, a decrease in the activity was observed (residual acetylation: 19.4 and 81.6%, respectively). Interestingly, replacement of the cyclohexanone moiety of RC56 with an *N*-benzyl-substituted piperidinone ring (as in **1s**) led to a decrease in the inhibitory activity (residual acetylation: 81.6%).

Interestingly, **1l**, **1o**, and **1q** showed slight activation of p300 activity. This phenomenon is not unusual. In our previous study of anacardic acid analogues for HAT inhibition, we similarly observed that certain HAT inhibitors showed an activating effect on the activities of p300 and p300/CBP-associated factor (PCAF).^[33] The exact mechanism is not clear. Possibly, some inhibitor analogues can bind to the HAT enzyme in a different conformation and, thus, work as agonists instead of antagonists.

Influence on cell-cycle regulation

Some of the compounds displaying activity against p300 were also tested in a “cell-based assay” to verify their capability to modify cell-cycle progression and to induce cell death. Leukemic monoblast U937 cells were treated with 50 μM of each compound (as reported in Figure 1) for 30 h. Next, the cell-cycle distribution and percentage of cell death were both analyzed. As shown in Figure 1, compound **1d** induced a weak G2 phase accumulation, whereas compounds **1a**, **1b**, **1f**, **1g**, and **1n** caused an increase in the percentage of cell numbers in the S phase.

Compounds **1b** and **1g** also showed a G1 block coupled with induction of cell death (Figure 1b) greater than that of RC56. Although compound **1i** did not change the cell-cycle distribution relative to the untreated control (ctrl), it induced weak cellular death ($\approx 8.5\%$). Notably, for compounds **1b**, **1d**, **1g**, and **1i** a strong correlation between the percentage of p300 inhibition (shown in Table 1) and the biological effect, reported here as the inhibition of proliferation and induction of cell death (Figure 1a,b), exists. The effects of compounds **1b** and **1g** seem to be very similar to the effects of RC56, as they show S phase accumulation and p300 IC_{50} values ranging from (38.9 ± 10.1) to $(8.1 \pm 2.1) \mu\text{M}$. However, for both compounds the percentage of cell death induced was greater than that obtained with RC56.

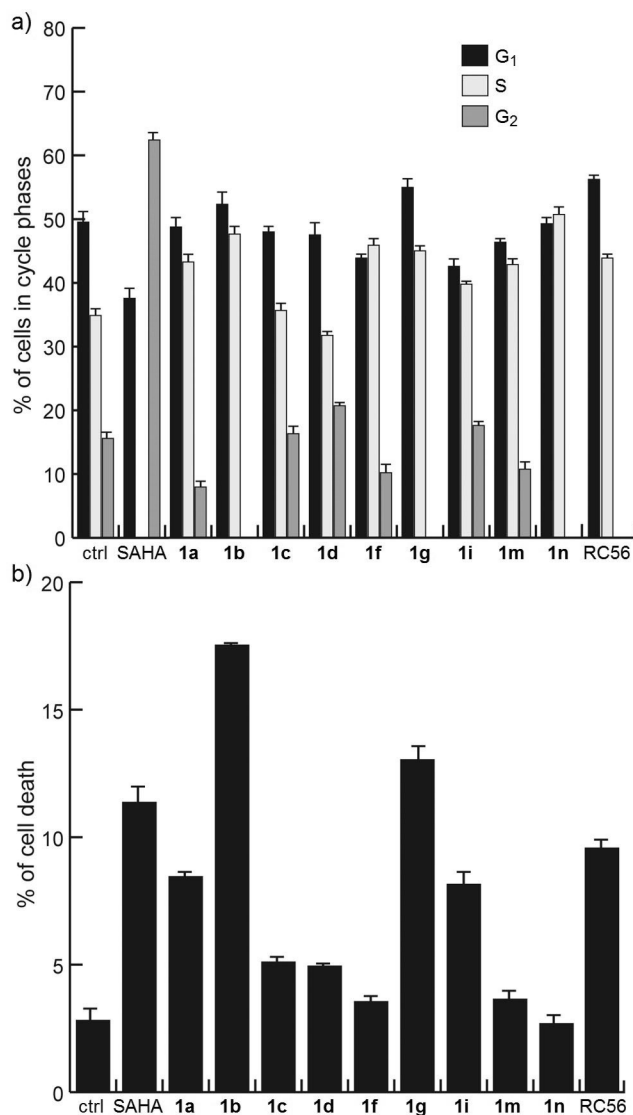


Figure 1. Cell-cycle distribution: a) percent of cells in cell-cycle phases and b) apoptosis induction. SAHA was used as a reference compound. Experiments were performed as independent biological triplicates. Error bars show the standard deviation of triplicates.

Molecular modeling study

An in-depth theoretical investigation of the interactions between p300 HAT and the best-emerged hits (i.e., **1i** and **1d**) was performed by means of induced-fit docking (IFD), molecular-mechanics-generalized Born/Poisson Boltzmann surface area (MM-GBSA) experiments, and molecular dynamics (MD) simulations. RC56 was analyzed as well as a reference compound.

Induced-fit docking experiments

Prior to docking, the compounds were built by using the Schrödinger Maestro interface^[34] and then submitted to the LigPrep utility,^[35] which rapidly produced low-energy 3D structures taking into account ionization states, tautomerism, stereochemistry, and ring conformations at the desired pH value.

For our study, the default pH range of 6 to 8 was kept. This analysis suggested that three molecules could exist in a neutral (N), monoanionic (M), or dianionic (D) form. Given that, nine different structures were obtained: RC56-N, RC56-M, and RC56-D; **1i**-N, **1i**-M, and **1i**-D; and **1d**-N, **1d**-M, and **1d**-D.

Then, docking experiments were performed by using the available crystal structure of the p300 HAT–Lys-CoA complex (PDB ID: 3BIY) and the IFD procedure,^[36–40] which took into account receptor flexibility upon ligand binding in an attempt to describe the binding mode of the inhibitor.

The IFD of the nine structures into the Lys-CoA binding domain generated a number of protein–ligand complexes, and the best ten scoring poses for each ionization state were retained and further analyzed. A comparison between the IFD conformations for each ligand in the different N, M, and D forms highlighted that all the docked positions could be clustered into two main distinct binding modes, A and B (Figure 2), independent of the ionization state of the inhibitor. Notably, a binding mode similar to A was also predicted for RC56 by Devipriya and Kumaradhas by using a different docking protocol.^[41]

Table 2. MM-GBSA ΔG values obtained for ligand–protein complexes selected by the IFD procedure.

Ligand in complex with HAT p300	ΔG [kcal mol ⁻¹]	
	Binding mode A	Binding mode B
RC56-N	–135.53	–127.95
RC56-M	–126.98	–120.15
RC56-D	–113.05	–117.82
1d -N	–136.46	–131.57
1d -M	–147.15	–128.09
1d -D	–120.63	–112.70
1i -N	–145.42	–137.21
1i -M	–154.93	–154.47
1i -D	–136.29	–111.96

MM-GBSA experiments

In an attempt to gain a more accurate ranking of the ligand docking poses, the ligand–protein complexes were rescored by using the MM-GBSA approach implemented in the Schrödinger's Maestro suite,^[41] and the results are summarized in Table 2.

Binding pose A was predicted to be the most favorable for both the RC56 and **1d** inhibitors, although the lowest-energy orientations were obtained for two different ionization states. Comparable MM-GBSA-dG values emerged for binding modes A and B of compound **1i**-M, which suggests that both poses could be reliable. It is also notable that for both binding modes the predicted binding energies reproduced the trend observed for the activity of the p300 HAT inhibitory, that is, the most interesting compound was **1i**, followed by **1d**, and finally RC56.

MD simulations

To assess the stability of binding modes A and B previously identified for compound **1i**-M and to identify the most ener-

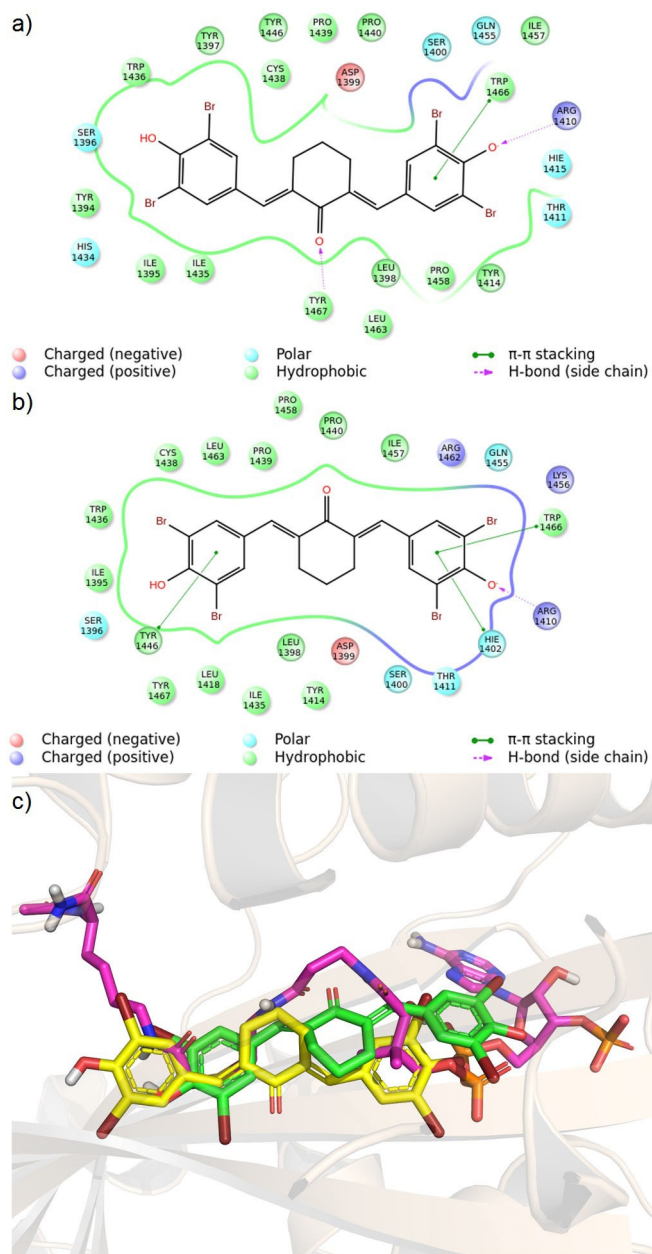


Figure 2. Alternative binding modes obtained for the cinnamoyl-based inhibitors at the p300 HAT domain. a, b) Schematic representations of the interactions between the protein and **1 i**, as a representative inhibitor, for binding modes A and B, respectively. c) Superimposition of the two binding modes (A: yellow, B: green) and the Lys-CoA (violet) substrate.

getically favorable structure, the two ligand–p300 HAT complexes were submitted to 28 ns molecular dynamics simulations in explicit solvent.

Superimposition of the final structures and the initial modeled structures showed that there were structural rearrangements within the binding sites of both complexes (see Figure S2, Supporting Information). Upon analyzing the dynamic behavior of the complex between p300 HAT and the ligand with binding mode A, we observed that the ligand tended to move more internally into the pocket to maximize the interac-

tion with Arg1410 (more than 110% occupancy), whereas the hydrogen bond with Tyr1467 was lost and the interactions with this residue were later mainly hydrophobic in nature. In its final pose, the ligand established hydrophobic interactions with Ile1457, Leu1463, Leu1398, Trp1466, Tyr1414, Ile1395, and Ile1435 and made a weak hydrogen bond in turn with the carbonyl backbone of Ser1396 or Trp1436 (Figure 3a,c). On the other hand, a marked rearrangement of the residues of the binding site was observed for complex B. In its final position, the ligand made polar interactions with Arg1410 (over 70% occupancy), Tyr1467 (67% occupancy), and the carbonyl backbone of Trp1436 (\approx 22% occupancy) (Figure 3b,d). Hydrophobic contacts were also detected between **1 i**-M and Trp1466, Tyr1414, Leu1398, Trp1436, Tyr1446, Ile1435, and Tyr1467. In this final complex, polar interactions as well as hydrophobic contacts were maximized. Accordingly, complex B was the most energetically favorable one in terms of free energy of binding between the ligand and protein, and the difference between the ΔG values of the two complexes was substantial ($\Delta\Delta G$ of $9.47 \text{ kcal mol}^{-1}$ in favor of complex B). The outputs of this study provide some useful information to aid the rational design of new cinnamoyl inhibitors of p300 HAT in the future.

Conclusions

Herein we reported a new series of cell-permeable cinnamoyl derivatives as inhibitors of p300 histone acetyltransferase (HAT) by addressing various structural modifications to our hit RC56 [2,6-bis(3-bromo-4-hydroxybenzylidene)cyclohexanone], involving both the benzylidene moiety and the central cyclohexanone portion. Among the tested derivatives, substituting the cyclohexanone moiety with another central ring highlighted a decreasing trend in the inhibition potency (see compounds **1 m**, **1 s**, and **2 a**), with the sole exception of the tetrahydrothiopyranone derivative, (3*Z*,5*Z*)-3,5-bis[(3-bromo-4-hydroxyphenyl)methylidene]thian-4-one (**1 n**), characterized by activity similar to that of RC56. As regards the cyclohexanone derivatives, replacing the bromine atom of RC56 with other halogen atoms (as in **1 b–d**) as well as a methyl group (as in **1 g**) led to derivatives with IC_{50} values similar to that of our hit. In particular, among them 2,6-bis(4-hydroxy-3-iodobenzylidene)cyclohexan-1-one (**1 d**) showed good inhibitory activity and was proven to be five times more active ($IC_{50} = 8.1 \mu\text{M}$) than the reference compound, though data arising from a cell-based assay showed a higher percentage of cell death induction in leukemic monoblast cells for (2*E*,6*E*)-2,6-bis[(3-fluoro-4-hydroxyphenyl)methylidene]cyclohexan-1-one (**1 b**) and (2*E*,6*E*)-2,6-bis[(4-hydroxy-3-methylphenyl)methylidene]cyclohexan-1-one (**1 g**) that was even greater than that obtained with RC56. Notably, (2*E*,6*E*)-2,6-bis[(3,5-dibromo-4-hydroxyphenyl)methylidene]cyclohexan-1-one (**1 i**), characterized by the introduction of a second bromine atom on the benzylidene portion, proved to be the most active compound with complete inhibition of p300 activity at $100 \mu\text{M}$ and an IC_{50} value [$(2.3 \pm 0.5) \mu\text{M}$] 15 times lower than that of RC56 [$(30.9 \pm 8.2) \mu\text{M}$] and, notably, very similar to that of C646 [$(3.6 \pm 0.6) \mu\text{M}$], which is regarded as one of the most potent p300 inhibitors. Furthermore, mo-

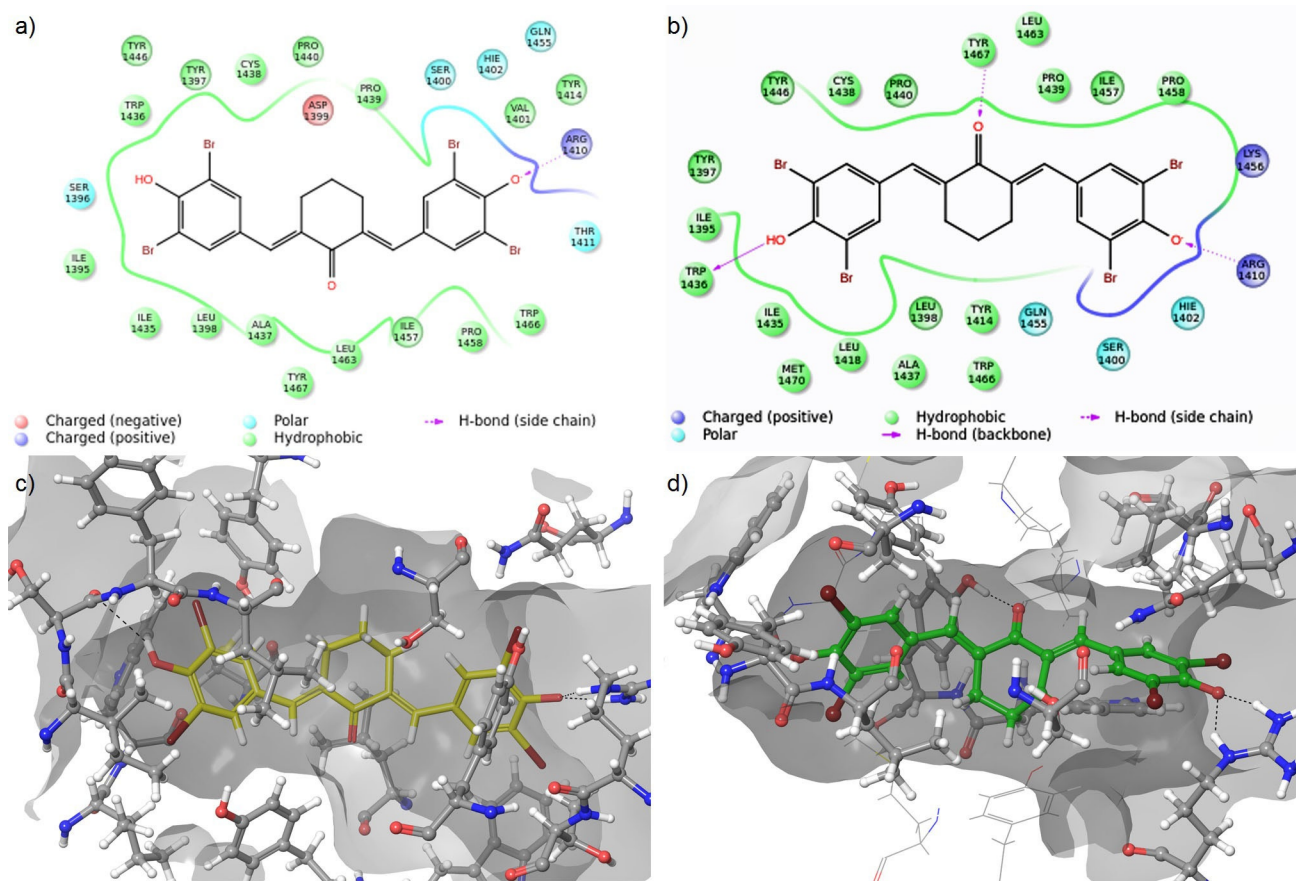


Figure 3. Minimized structures resulting from MD simulations of **1i**-M/p300 complexes A and B. a, b) 2D schematic representations of the interactions between the protein and **1i** for binding modes A and B, respectively. c, d) 3D perspectives of the same information. For the sake of clarity, only a few key residues are labeled and hydrogen-bonding interactions are represented by black dashed lines.

lecular-modeling studies highlighted the main structural features involved in the formation of a ligand–protein complex for the key role played by the phenolate moieties in establishing a salt bridge with the amino acid residues at the active site, as stated by the biological data (indeed, substitution of the hydroxy groups with bromine atoms in derivative **1h** led to a remarkable decrease in inhibition potency). Interestingly, two distinct binding modes within the p300 HAT domain, one for RC56 and **1d** and another for **1i**, were identified, which suggests that the introduction of a second bromine atom may have caused a rearrangement of the inhibitor within the enzymatic binding site.

In conclusion, this study provided useful insight for the future development of novel small molecules as p300 HAT inhibitors. In particular, **1i** as a low-micromolar inhibitor represents a very interesting compound, additional rational modifications of which might represent a line of inquiry for antitumor and antiviral vanguard chemotherapies.

Experimental Section

General procedures

Melting points were determined with a Büchi 530 capillary apparatus and are uncorrected. The purities of the compounds were

always > 95%, as determined by high-pressure liquid chromatography (HPLC). HPLC analyses were performed with a Shimadzu LC-10AD VP CTO-10AC VP by using a Discovery Bio Wide Pore C18 (10 cm × 4.6 mm, 3 μm) column. Infrared (IR) spectra were recorded with a PerkinElmer Spectrum-one spectrophotometer. ¹H NMR spectra were recorded with a Bruker AC 400 spectrometer. Merck silica gel 60 F₂₅₄ plates were used for analytical TLC (thin-layer chromatography). Developed plates were visualized by UV light. Column chromatography was performed on silica gel (Merck; 70–230 mesh). Concentration of solutions upon completion of the reactions and after extraction was performed with a rotary evaporator operating at reduced pressure. Analytical results agreed to within ± 0.40% of the theoretical values. [D₆]DMSO (99.9%, code 44 139-2) and CDCl₃ (98.8%, code 41 675-4) of isotopic purity (Aldrich) were used. Solvents were reagent grade and, if necessary, were purified and dried by standard methods. Organic solutions were dried with anhydrous sodium sulfate (Merck).

Microwave reactions were conducted by using a CEM Discover system unit (CEM. Corp., Matthews, NC). The machine consisted of a continuous focused microwave-power delivery system with an operator-selectable power output of 0 to 300 W. The temperature of the contents of the vessel was monitored by using a calibrated infrared temperature control mounted under the reaction vessel. All experiments were performed by using a stirring option, whereby the contents of the vessel were stirred by means of a rotating magnetic plate located below the floor of the microwave cavity and a Teflon-coated magnetic stir bar in the vessel.

Final compounds **1a–s** and **2a** were synthesized according to a reported procedure^[29,31] and described in Scheme 1. Spectroscopic, chemical, and physical data of compounds **1a**, **1b**, **1e**, **1g**, **1i**, **1l**, and **1n–r** are already described in the literature.^[29,31,42] Spectroscopic, chemical, and physical data of derivatives **1c**, **1d**, **1f**, **1h**, **1j**, **1k**, **1m**, and **1s** are reported below. Experimental procedures, yields, melting points, recrystallization solvents, IR spectroscopy data, and ¹H NMR spectroscopy data of derivatives **2a** and **3f** are reported below.

Synthesis

6-Hydroxy-1,1'-biphenyl-3-carboxaldehyde (3f): Phenylboronic acid (15.76 mmol), tetrakis(triphenylphosphine)palladium(0) (0.77 mmol), Ba(OH)₂·8H₂O (19.73 mmol), and H₂O (22.6 mL) were sequentially added to a solution of **3k** (13.15 mmol) in 1,2-dimethoxyethane (180 mL). The mixture was stirred at reflux under an argon atmosphere for 4 h. The reaction was quenched with water, and the mixture was extracted with ethyl acetate. The combined organic layers were washed with brine, dried (Na₂SO₄), filtered, and concentrated under reduced pressure to give the crude product as a yellow oil (6 g). Purification of the crude product was performed by column chromatography on silica gel (chloroform/ethyl acetate=3:1) to afford the pure product as a yellow oil (880 mg, 32%). Spectroscopic data as per Zhao et al.^[43]

2,6-Bis(3-chloro-4-hydroxybenzylidene)cyclohexan-1-one (1c): Yield: 79 mg (40%); oil; ¹H NMR (400 MHz, [D₆]DMSO): δ = 1.72–1.75 (m, 2H, CH₂), 2.85 (t, *J*_{CH₂} = 8 Hz, 4H, CH₂), 7.04 (d, *J*_o = 8.4 Hz, 2H), 7.41 (d, *J*_o = 8.4 Hz, *J*_m = 1.8 Hz, 2H), 7.50 (s, 2H, =CH–), 7.54 (d, *J*_m = 1.8 Hz, 2H), 10.4 ppm (brs, 2H, OH); IR (KBr): $\tilde{\nu}$ = 3401 (OH), 1639 cm⁻¹ (C=O); elemental analysis calcd (%) for C₂₀H₁₆Cl₂O₃ (375.25): C 64.02, H 4.30, Cl 18.89; found: C 63.70, H 4.02, Cl 18.55.

2,6-Bis(4-hydroxy-3-iodobenzylidene)cyclohexan-1-one (1d): Yield: 98 mg (22%); mp: 183 °C (methanol); ¹H NMR (400 MHz, [D₆]DMSO): δ = 1.71–1.74 (m, 2H, CH₂), 2.84 (t, *J*_{CH₂} = 8 Hz, 4H, CH₂), 6.95 (d, *J*_o = 8.4 Hz, 2H), 7.43 (d, *J*_o = 8.4 Hz, *J*_m = 2.1 Hz, 2H), 7.48 (s, 2H, =CH–), 7.86 (d, *J*_m = 2.1 Hz, 2H), 11 ppm (brs, 2H, OH); IR (KBr): $\tilde{\nu}$ = 3223 (OH), 1651 cm⁻¹ (C=O); elemental analysis calcd (%) for C₂₀H₁₆I₂O₃ (558.15): C 43.04, H 2.89, I 45.47; found: C 42.68, H 2.58, I 45.21.

2,6-Bis(6-hydroxy-1,1'-biphenyl-3-yl)methylene)cyclohexan-1-one (1f): Yield: 125 mg (42%); oil; ¹H NMR (400 MHz, [D₆]DMSO): δ = 1.73–1.76 (m, 2H, CH₂), 2.91 (t, *J*_{CH₂} = 8 Hz, 4H, CH₂), 7.05 (d, *J*_o = 8 Hz, 2H), 7.31 (d, *J*_o = 8 Hz, 2H), 7.42–7.46 (m, 8H), 7.86–7.89 (m, 6H), 10.1 ppm (brs, 2H, OH); IR (KBr): $\tilde{\nu}$ = 3223 (s, br), 1664 cm⁻¹ (C=O); elemental analysis calcd (%) for C₃₂H₂₆O₃ (458.55): C 83.82, H 5.72; found: C 83.60, H 6.08.

2,6-Bis(3,4-dibromobenzylidene)cyclohexan-1-one (1h): Yield: 111 mg (36%); mp: 165 °C (benzene); ¹H NMR (400 MHz, [D₆]DMSO): δ = 1.72–1.75 (m, 2H, CH₂), 2.86 (t, *J*_{CH₂} = 8 Hz, 4H, CH₂), 7.43 (d, *J*_o = 8.3 Hz, *J*_m = 1.9 Hz, 2H), 7.54 (s, 2H, =CH–), 7.83 (d, *J*_o = 8.3 Hz, 2H), 7.91 ppm (d, *J*_m = 1.8 Hz, 2H); IR (KBr): $\tilde{\nu}$ = 1661 cm⁻¹ (C=O); elemental analysis calcd (%) for C₂₀H₁₄Br₄O (589.94): C 40.72, H 2.39, Br 54.18; found: C 40.37, H 1.99, Br 53.89.

2,6-Bis(3-chloro-5-fluoro-4-hydroxybenzylidene)cyclohexan-1-one (1j): Yield: 90 mg (22%); mp: 160–161 °C (toluene); ¹H NMR (400 MHz, [D₆]DMSO): δ = 1.73–1.76 (m, 2H, CH₂), 2.86 (t, *J*_{CH₂} = 8 Hz, 4H, CH₂), 7.42–7.47 (m, 6H), 10.97 ppm (brs, 2H, OH); IR (KBr): $\tilde{\nu}$ = 1664 cm⁻¹ (C=O); elemental analysis calcd (%) for C₂₀H₁₄Cl₂F₂O₃ (411.23): C 58.42, H 3.43, Cl 17.24, F 9.24; found: C 58.71, H 3.22, Cl 17.61, F 9.49.

5,5'-[(5-Carboxy-2-oxocyclohexane-1,3-diylidene)bis(methanylylidene)]bis(2-hydroxybenzoic acid) (1k): Yield: 131 mg (40%); mp: 170–173 °C (toluene); ¹H NMR (400 MHz, [D₆]DMSO): δ = 2.80–2.82 (m, 2H, CH₂), 3.06–3.09 (m, 2H, CH₂), 7.06 (d, *J*_o = 8.6 Hz, 2H), 7.61 (s, 2H, =CH–), 7.72 (d, *J*_o = 8.6 Hz, *J*_m = 1.2 Hz, 2H), 7.98 (d, *J*_m = 1.2 Hz, 2H), 12–13 ppm (brs, 2H, OH); IR (KBr): $\tilde{\nu}$ = 3500–2500 (OH), 1650 cm⁻¹ (C=O); elemental analysis calcd (%) for C₂₃H₁₈O₉ (438.38): C 63.02, H 4.14; found: C 63.34, H 3.89.

2,5-Bis[(E)-3-bromo-4-hydroxybenzylidene]cyclopentan-1-one (1m): Yield: 110 mg (33%); mp: 154–156 °C (toluene); ¹H NMR (400 MHz, [D₆]DMSO): δ = 2.99 (s, 4H, CH₂), 6.89 (d, *J*_o = 8.6 Hz, 2H), 7.42 (s, 2H, =CH–), 7.58 (d, *J*_o = 8.6 Hz, *J*_m = 1.2 Hz, 2H), 7.91 (d, *J*_m = 1.2 Hz, 2H), 10.2 ppm (brs, 2H, OH); IR (KBr): $\tilde{\nu}$ = 3229 (OH), 1671 cm⁻¹ (C=O); elemental analysis calcd (%) for C₁₉H₁₄Br₂O₃ (450.12): C 50.70, H 3.14, Br 35.50; found: C 50.98, H 3.00, Br 35.29.

1-Benzyl-3,5-bis[(E)-3-bromo-4-hydroxybenzylidene]piperidin-4-one (1s): Yield: 94 mg (38%); mp: 180 °C (dioxane/diethyl ether); ¹H NMR (400 MHz, [D₆]DMSO): δ = 3.42 (s, 4H, CH₂ piperidinone), 3.57 (s, 2H, CH₂Bz), 6.69 (d, *J*_o = 7.5 Hz, *J*_m = 1.2 Hz, 2H), 7.22–7.31 (m, 5H, Ph), 7.43 (d, *J*_o = 7.5 Hz, *J*_m = 1.2 Hz, 2H), 7.59 (s, 2H, =CH–), 8.26 (d, *J*_m = 1.2 Hz, 2H), 9.98 ppm (brs, 2H, OH); IR (KBr): $\tilde{\nu}$ = 3225 (OH), 1674 cm⁻¹ (C=O); elemental analysis calcd (%) for C₂₁H₁₉Br₂NO₃ (493.19): C 51.14, H 3.88, Br 32.40, N 2.84; found: C 51.41, H 3.70, Br 32.79, N 2.99.

4,4'-(2-Hydroxycyclohexane-1,3-diylidene)bis(methanylylidene)-bis(2-bromophenol) (2a): A solution of RC56 (0.75 g, 1.63 mmol) in anhydrous THF (53 mL) was added dropwise to a well-stirred suspension of lithium aluminum hydride (50 mmol) in anhydrous THF (494 mL) cooled to 0 °C. The mixture was then stirred at room temperature for 4 h. Crushed ice was added to the mixture until the formation of hydrogen vapors stopped. The produced aluminum hydroxide was filtered off by means of a Büchner filter, and the resulting solution was evaporated under reduced pressure to give the crude product (0.74 g). Purification of the crude product by column chromatography on silica gel (chloroform) gave the pure product as a yellow oil (250 mg, 32%). ¹H NMR (400 MHz, [D₆]DMSO): δ = 1.73–1.76 (m, 2H, CH₂), 2.84–2.87 (m, 4H, CH₂), 7.02 (d, *J*_o = 8.44 Hz, 2H), 7.41 (d, *J*_o = 8.50 Hz, 2H), 7.49 (s, 1H, =CH–), 7.68 (s, 1H, =CH–), 10.79 ppm (brs, 1H, OH); IR (KBr): $\tilde{\nu}$ = 3468 (OH), 3234 cm⁻¹ (OH); elemental analysis calcd (%) for C₂₀H₁₈Br₂O₃ (466.16): C 51.53, H 3.89, Br 34.28; found: C 51.69, H 4.13, 33.92.

Biological methods

Enzyme assays: The expression and purification of the tag-free recombinant human p300 HAT domain enzyme (residues 1287–1666) was done by using the method developed by Cole's laboratory.^[44] The standard filter binding assay was used to measure the acetyltransferase activity of p300 in the presence of various inhibitors. A histone H3 peptide containing the amino-terminal 20 residues (H3-20) was used as the substrate, and the concentration was set at 100 μM. 1 μM [¹⁴C]-Ac-CoA was used as the acetyl donor. The reaction buffer contained 50 mM 4-(2-hydroxyethyl)-1-piperazineethanesulfonic acid (HEPES; pH 8), 1 mM ethylenediaminetetraacetic acid (EDTA), and 0.5 mM dithiothreitol (DTT). The reaction time was 6 min at 30 °C. An aliquot (30 μL) comprising the inhibitor, peptide, and cofactor was incubated at 30 °C for 5 min, which was followed by the addition of p300 (final at 0.025 μM). After incubating for 6 min, the reaction was quenched by spreading the reaction mixture (20 μL) over a Whatman P81 filter disc. Once the filter discs were dried, they were washed with 50 mM NaHCO₃ (pH 9.0, 3×) and redried. The acetylated products were quantified by using a Mi-

croBeta2 (PerkinElmer) after the addition of scintillation cocktail. The enzymatic reaction was controlled in the initial linear phase, with a typical conversion yield of less than 20%. Each measurement was done at least in duplicate with errors less than 20%.

Cell-based assays

Drugs: SAHA (Merck, Readington, NJ, USA) was dissolved in DMSO and used at 5 μM concentration.

Cell lines: U937 cells (ATCC) were cultured by using standard procedures in RPMI (Euroclone) supplemented with 10% fetal bovine serum (FBS; Sigma), 50 $\mu\text{g mL}^{-1}$ penicillin–streptomycin, and 2 mM glutamine.

Cell-cycle analysis: The cells were plated (2×10^5 cells mL^{-1}) and stimulated for 30 h with compounds at 50 μM . Treated and untreated U937 cells were harvested and resuspended in staining solution containing RNaseA, PI (50 $\mu\text{g mL}^{-1}$), sodium citrate (0.1%), and NP40 (0.1%) in cold phosphate-buffered saline (PBS) for 30 min in the dark. Cell-cycle distribution was assessed with a FACScalibur flow cytometer by using the Cell Quest software (Becton Dickinson, Milan, Italy). ModFit LT version 3 Software (Verity, Topsham, ME, USA) was used for analysis.

Cell-death analysis: After stimulation with selected compounds for 30 h at 50 μM , treated and untreated U937 cells were collected in 0.1% sodium citrate and 50 $\mu\text{g mL}^{-1}$ PI. After incubating for 30 min, the percentage of cells with sub-G1 DNA was analyzed with FACS (FACScalibur; BD Biosciences, San Jose, CA).

Molecular modeling studies

Protein and ligand preparation: The crystal structure of p300 HAT domain in complex with a bisubstrate inhibitor, that is, Lys-CoA, was retrieved from the RCSB Protein Data Bank (PDB ID: 3BIY)^[18] and was used as a target for the modeling studies. The inhibitor and the water molecules were deleted, and the Schrödinger Protein Preparation Wizard^[45] was then used to obtain a satisfactory starting structure for docking studies. This facility is designed to ensure chemical correctness and to optimize a protein structure for further analysis. In particular, hydrogen atoms were added, and bond orders and charges were assigned; the orientation of the hydroxy groups on Ser, Thr, and Tyr; the side chains of the Asn and Gln residues; and the protonation state of the His residues were optimized. Steric clashes were relieved by performing a small number of minimization steps not intended to minimize the system completely. In our study, the minimization (OPLS force field) was stopped if the RMSD of the non-hydrogen atoms reached 0.30 Å. The analyzed compounds, RC56, **1d**, and **1i**, were constructed by using Maestro 9.9^[34] and were then submitted to the LigPrep module^[35] by using the default parameters.

Docking studies: The IFD protocol,^[36–39] developed by Schrödinger, was employed to predict the ligand binding modes and concomitant structural changes in the p300 HAT receptor. The prepared protein structure was used to generate the receptor grid, which was centered on the crystallographic position of the Lys-CoA substrate; afterward, the simulations were run by setting the “Extended Sampling” protocol and by refining residues within 6 Å of all ligand poses. All the other parameters were left at the default values. Binding free-energy estimates were evaluated for the top-docked complexes by using MM-GBSA calculations.

MD simulations: Molecular dynamics (MD) simulations were performed through the use of the AMBER 12 suite of programs^[46] and

the ff03.r1 force field. An appropriate number of counterions was added to neutralize the system, and complexes were placed in an octagonal box of TIP3P water molecules. The distance between the box walls and the protein was set to 10 Å. MD runs were performed with a protocol previously validated.^[47–49] Before MD simulation, two stages of energy minimization were performed to remove bad contacts. In the first stage, we kept the protein fixed with a constraint of 500 kcal mol^{-1} and we minimized the positions of the water molecules. Then, in the second stage, we minimized the entire system by applying a constraint of 10 kcal mol^{-1} on the α carbon atoms. MD trajectories were run by using the minimized structure as the starting input. Constant volume simulations were performed for 50 ps, during which time the temperature was raised from 0 to 300 K by using the Langevin dynamics method. Then, 150 ps of constant-pressure MD simulations were performed at 300 K in three steps of 50 ps each. During the three periods of this second stage, the α carbon atoms were blocked with harmonic force constants of 10, 5, and 1 kcal $\text{mol}^{-1} \cdot \text{Å}$, respectively. Finally a 28 ns MD simulation without restraint was run at a constant temperature of 300 K and a constant pressure of 0.1 MPa. The RMSDs of the α -carbon atoms were then calculated throughout the simulations with respect to the starting structure for both systems. After the first nanosecond, both 1i-M/p300 HAT complexes reached an equilibrium state, and stable RMSDs were detected during the remaining time of the MD simulations (see Figure S1).

Acknowledgements

We thank FIRB RBF10ZJQT_003, EU (Blueprint High-Impact Project, no. 28251) and MIUR (PRIN 2012ZHN9YH, 20152TE5PK), EPIGEN (MIUR-CNR), AIRC (17217), POR Campania FESR 2007–2013-MOVIE (B25C13000240007), and COST EPICHEM BIO CM1406. Y.G.Z. was supported by American Heart Association (AHA) grant 12GRNT12070056 and US National Institutes of Health (NIH) grant R01GM086717.

Conflict of interest

The authors declare no conflict of interest.

Keywords: antitumor agents · drug discovery · medicinal chemistry · structure–activity relationships · transferases

- [1] R. Eckner, M. E. Ewen, D. Newsome, M. Gerdes, J. A. DeCaprio, J. B. Lawrence, D. M. Livingston, *Genes Dev.* **1994**, *8*, 869–884.
- [2] D. E. Sterner, S. L. Berger, *Microbiol. Mol. Biol. Rev.* **2000**, *64*, 435–459.
- [3] a) A. C. Brown, V. Nair, M. Allday, *J. Virol.* **2012**, *86*, 1683–1695; b) B. Alberter, A. Ensser, *J. Virol.* **2007**, *81*, 2524–2530.
- [4] M. T. S. Robles, C. Shivalila, J. Wano, S. Sorrells, A. Roos, J. M. Pipas, *J. Virol.* **2013**, *87*, 13499–13509.
- [5] S. J. Noh, M. J. Kang, K. M. Kim, J. S. Bae, H. S. Park, W. S. Moon, M. J. Chung, H. Lee, D. G. Lee, K. Y. Jang, *Pathology* **2013**, *45*, 574–580.
- [6] S. K. Kurdistani, S. Tavazoie, M. Grunstein, *Cell* **2004**, *117*, 721–733.
- [7] J. H. Chen, Q. Li, *Epigenetics* **2011**, *6*, 957–961.
- [8] Y. Zheng, X. Yao, *Viruses* **2013**, *5*, 1787–1801.
- [9] M. Arif, G. V. P. Kumar, C. Narayana, T. K. Kundu, *J. Phys. Chem. B* **2007**, *111*, 11877–11879.
- [10] N. G. Iyer, J. Xian, S.-F. Chin, A. J. Bannister, Y. Daigo, S. Aparicio, T. Kouzarides, C. Caldas, *Oncogene* **2007**, *26*, 21–29.
- [11] P.-P. Wong, A. Pickard, D. J. McCance, *PLoS One* **2010**, *5*, e8369.
- [12] a) R. K. Vempati, R. S. Jayani, D. Notani, A. Sengupta, S. Galande, D. Haldar, *J. Biol. Chem.* **2010**, *285*, 28553–28564; b) I. V. Getun, Z. Wu, M.

- Falahi, S. Ouizem, Q. Liu, W. Li, R. Costi, W. R. Roush, J. L. Cleveland, P. R. J. Bois, *Mol. Cell. Biol.* **2017**, *37*, e00942-15.
- [13] N. G. Iyer, S.-F. Chin, H. Ozdag, Y. Daigo, D.-E. Hu, M. Cariati, K. Brindle, S. Aparicio, C. Caldas, *Proc. Natl. Acad. Sci. USA* **2004**, *101*, 7386–7391.
- [14] a) N. G. Iyer, H. Ozdag, C. Caldas, *Oncogene* **2004**, *23*, 4225–4231; b) F. Wang, C. B. Marshall, M. Ikura, *Cell. Mol. Life Sci.* **2013**, *70*, 3989–4008.
- [15] X. Y. Zhu, C. S. Huang, Q. Li, R. M. Chang, Z. B. Song, W. Y. Zou, *Mol. Pain* **2012**, *8*, 84.
- [16] L. M. Valor, J. Viosca, J. P. Lopez-Atalaya, A. Barco, *Curr. Pharm. Des.* **2013**, *19*, 5051–5064.
- [17] K. Yasufumi, S. Yoichi, H. Koji, M. Tatsuya, *Biol. Pharm. Bull.* **2013**, *36*, 13–17.
- [18] X. Liu, L. Wang, K. Zhao, P. R. Thompson, Y. Hwang, R. Marmorstein, P. A. Cole, *Nature* **2008**, *451*, 846–850.
- [19] J. Maksimoska, D. Segura-Pena, P. A. Cole, R. Marmorstein, *Biochemistry* **2014**, *53*, 3415–3422.
- [20] F. J. Dekker, H. J. Haisma, *Drug Discovery Today* **2009**, *14*, 942–948.
- [21] K. Balasubramanyam, V. Swaminathan, A. Ranganathan, T. K. Kundu, *J. Biol. Chem.* **2003**, *278*, 19134–19140.
- [22] M. G. Marcu, Y.-J. Jung, S. Lee, E.-J. Chung, M. J. Lee, J. Trepel, L. Neckers, *Med. Chem.* **2006**, *2*, 169–174.
- [23] S. A. Maddox, C. S. Watts, V. Doyère, G. E. Schafe, *PLoS One* **2013**, *8*, e54463.
- [24] K.-C. Choi, M. G. Jung, Y.-H. Lee, J. C. Yoon, S. H. Kwon, H.-B. Kang, M.-J. Kim, J.-H. Cha, Y. J. Kim, W. J. Jun, J. M. Lee, H.-G. Yoon, *Cancer Res.* **2009**, *69*, 583–592.
- [25] K. C. Ravindra, B. R. Selvi, M. Arif, B. A. A. Reddy, G. R. Thanuja, S. Agrawal, S. K. Pradhan, N. Nagashayana, D. Dasgupta, T. K. Kundu, *J. Biol. Chem.* **2009**, *284*, 24453–24464.
- [26] Y. Zheng, K. Balasubramanyam, M. Cebrat, D. Buck, F. Guidez, A. Zelent, R. M. Alani, P. A. Cole, *J. Am. Chem. Soc.* **2005**, *127*, 17182–17183.
- [27] X.-n. Gao, J. Lin, Q.-y. Ning, L. Gao, Y.-s. Yao, J.-h. Zhou, Y.-h. Li, L.-l. Wang, L. Yu, *PLoS One* **2013**, *8*, e55481.
- [28] L. Stimson, M. G. Rowlands, Y. M. Newbatt, N. F. Smith, F. I. Raynaud, P. Rogers, V. Bavetsias, S. Gorsuch, M. Jarman, A. Bannister, T. Kouzarides, E. McDonald, P. Workman, G. W. Aherne, *Mol. Cancer Ther.* **2005**, *4*, 1521–1532.
- [29] R. Costi, R. Di Santo, M. Artico, G. Miele, P. Valentini, E. Novellino, A. Cereseto, *J. Med. Chem.* **2007**, *50*, 1973–1977.
- [30] M. Toth, I. M. Boros, E. Balint, *Cancer Sci.* **2012**, *103*, 659–669.
- [31] R. Costi, R. Di Santo, M. Artico, S. Massa, R. Ragno, R. Loddo, M. La Colla, E. Tramontano, P. La Colla, A. Pani, *Bioorg. Med. Chem.* **2004**, *12*, 199–215.
- [32] M. Azoulay, G. Tuffin, W. Sallem, J.-C. Florent, *Bioorg. Med. Chem.* **2006**, *16*, 3147–3149.
- [33] M. Ghizzoni, J. Wu, T. Gao, H. J. Haisma, F. J. Dekker, G. Y. Zheng, *Eur. J. Med. Chem.* **2012**, *47*, 337–344.
- [34] Maestro, Version 9.9, Schrödinger LLC, New York, NY, **2014**.
- [35] LigPrep, Version 3.1, Schrödinger LLC, New York, NY, **2014**.
- [36] Schrödinger Suite 2014-3 Induced Fit Docking protocol, Glide Version 6.4, Schrödinger LLC, New York, NY, **2014**; Prime Version 3.7, Schrödinger LLC, New York, NY, **2014**.
- [37] R. Farid, T. Day, R. A. Friesner, R. A. Pearlstein, *Bioorg. Med. Chem.* **2006**, *14*, 3160–3173.
- [38] W. Sherman, T. Day, M. P. Jacobson, R. A. Friesner, R. Farid, *J. Med. Chem.* **2006**, *49*, 534–553.
- [39] W. Sherman, H. S. Beard, R. Farid, *Chem. Biol. Drug Des.* **2006**, *67*, 83–84.
- [40] M. L. Barreca, N. Iraci, L. De Luca, A. Chimirri, *ChemMedChem* **2009**, *4*, 1446–56.
- [41] B. Devipriya, P. Kumaradhas, *Chem.-Biol. Interact.* **2013**, *204*, 153–165.
- [42] a) M. Artico, R. Di Santo, R. Costi, E. Novellino, G. Greco, S. Massa, E. Tramontano, M. E. Marongiu, A. De Montis, P. La Colla, *J. Med. Chem.* **1998**, *41*, 3948–3960; b) H. Ligeret, G. Barthélémy, S. B. Doulikas, P.-A. Carrupt, J.-P. Tillement, S. Labidalle, D. Morin, *FEBS Lett.* **2004**, *569*, 37–42; c) M. A. Osman, A. Othman, M. A. Abd-Alla, *Polymer* **1992**, *33*, 52–56; d) A. Mai, D. Cheng, M. T. Bedford, S. Valente, A. Nebbioso, A. Perrone, G. Brosch, G. Sbardella, F. De Bellis, M. Miceli, L. Altucci, *J. Med. Chem.* **2008**, *51*, 2279–2290.
- [43] J. Zhao, Q. Zhang, L. Liu, Y. He, J. Li, Q. Zhu, *Org. Lett.* **2012**, *14*, 5362–5365.
- [44] P. R. Thompson, D. Wang, L. Wang, M. Fulco, N. Pediconi, D. Zhang, W. An, Q. Ge, R. G. Roeder, J. Wong, M. Levreno, V. Sartorelli, R. J. Cotter, P. A. Cole, *Nat. Struct. Mol. Biol.* **2004**, *11*, 308–315.
- [45] Schrödinger Suite 2014-3 Protein Preparation Wizard, Epik Version 2.9, Schrödinger LLC, New York, NY, **2014**; Impact Version 6.4, Schrödinger LLC, New York, NY, **2014**; Prime Version 3.7, Schrödinger LLC, New York, NY, **2014**.
- [46] D. A. Case, T. A. Darden, T. E. Cheatham III, C. L. Simmerling, J. Wang, R. E. Duke, R. Luo, R. C. Walker, W. Zhang, K. M. Merz, B. Roberts, S. Hayik, A. Roitberg, G. Seabra, J. Swails, A. W. Götz, I. Kolossváry, K. F. Wong, F. Paesani, J. Vanicek, R. M. Wolf, J. Liu, X. Wu, S. R. Brozell, T. Steinbrecher, H. Gohlke, Q. Cai, X. Ye, J. Wang, M. J. Hsieh, G. Cui, D. R. Roe, D. H. Mathews, M. G. Seetin, R. Salomon-Ferrer, C. Sagui, V. Babin, T. Luchko, S. Gusarov, A. Kovalenko, P. A. Kollman, AMBER 12, University of California, San Francisco, CA, **2012** (<http://ambermd.org/>).
- [47] C. Tintori, N. Veljkovic, V. Veljkovic, M. Botta, *Proteins Struct. Funct. Bioinf.* **2010**, *78*, 3396–3408.
- [48] T. Tuccinardi, F. Manetti, S. Schenone, A. Martinelli, M. Botta, *J. Chem. Inf. Model.* **2007**, *47*, 644–655.
- [49] C. Granchi, S. Roy, S. A. De Simone, I. Salvetti, T. Tuccinardi, A. Martinelli, M. Macchia, M. Lanza, L. Betti, G. Giannaccini, A. Lucacchini, E. Giovannetti, R. Sciarillo, G. J. Peters, F. Minutolo, *Eur. J. Med. Chem.* **2011**, *46*, 5398–5407.

Manuscript received: January 19, 2017

Revised manuscript received: March 17, 2017

Accepted manuscript online: March 27, 2017

Version of record online: April 12, 2017